Normal-state properties of spin-orbit-coupled Fermi gases in the upper branch of the energy spectrum

Xiao-Lu Yu, Shang-Shun Zhang, and Wu-Ming Liu
Beijing National Laboratory for Condensed Matter Physics, Institute of Physics, Chinese Academy of Sciences, Beijing 100190, China
(Received 10 December 2012; published 29 April 2013)

We investigate normal-state properties of spin-orbit-coupled Fermi gases with repulsive s-wave interaction, in the absence of molecule formation, i.e., in the so-called "upper branch." Within the framework of random-phase approximation, we derive analytical expressions for the quasiparticle lifetime τ_s, the effective mass m_s^*, and the Green's function renormalization factor Z_s in the presence of Rashba spin-orbit coupling. In contrast to spin-orbit-coupled electron gas with Coulomb interaction, we show that the modifications are dependent on the Rashba band index s and occur in the first order of the spin-orbit-coupling strength. We also calculate experimental observables such as spectral weight, density of state, and specific heat, which exhibit significant differences from their counterparts without spin-orbit coupling. We expect our microscopic calculations of these Fermi-liquid parameters would have immediate applications to the spin-orbit-coupled Fermi gases in the upper branch of the energy spectrum.

DOI: 10.1103/PhysRevA.87.043633 PACS number(s): 03.75.Ss, 05.30.Fk, 67.85.Lm

I. INTRODUCTION

Motivated by the recent success on the evidence of Stoner ferromagnetism for the repulsive Fermi gas in the upper branch of the energy spectrum [1], there has been increasing interest in the nature of uncondensed Fermi gas (free of molecules) within the repulsively interacting regime [2], which naturally becomes the well-controlled platform for simulating Landau Fermi liquid. Much of the interest in ultracold atomic gases comes from their amazing tunability. A wide range of atomic physics and quantum optics technology provides unprecedented manipulation of a variety of intriguing quantum phenomena. Based on the Berry phase effect [3] and its non-Abelian generalization [4], Spielman's group at the National Institute of Standards and Technology has successfully generated a synthetic external Abelian or non-Abelian gauge potential coupled to neutral atoms. Recent experiments have realized the atomic ^{40}K [5] or ^{6}Li [6] gases with spin-orbit coupling (SOC). These achievements will open a whole new avenue in cold atom physics [7–10].

The effect of SOC in fermionic systems has consequently become an important issue in recent years and has attracted a great deal of attention to ultracold Fermi gases. Most of the existing works are devoted to the effect of SOC on the superfluid state with negative s-wave scattering length [11–13] and to the Bardeen-Cooper-Schrieffer (BCS) to Bose-Einstein condensation (BEC) crossover [14–17]. Furthermore, SOC gives rise to a variety of topological phases, such as the quantum spin Hall state and the topological superfluid [18–21]. In addition to the study of the SOC effect on these symmetry-breaking or topological phases, the normal state contains various potential instabilities and deserves attention. The consideration of SOC systems in the framework of Fermi-liquid theory is therefore desirable. As is well known, Landau's Fermi-liquid theory provides a phenomenological approach to describe the properties of strongly interacting fermions. Fermi-liquid parameters characterizing the renormalized many-body effective interactions have to be determined through experimental results.

The purpose of this paper is to study key normal-state properties of two-dimensional (2D) Fermi gases with SOC in the repulsive regime—their quasiparticle lifetime, effective mass, and Green's function renormalization factor. Following previous studies of Landau's Fermi-liquid theory including SOC [22,23], we attempt to build a microscopic foundation of phenomenological parameters. Therefore within the framework of random-phase approximation (RPA), we derive analytical expressions for the quasiparticle lifetime τ_s, the effective mass m_s^*, and the Green's function renormalization factor Z_s for a 2D Fermi gas with repulsive s-wave interaction in the presence of Rashba SOC. To make contact with current experiments directly, we also calculate experimental observables such as spectral weight, density of state, and specific heat and discuss their corresponding experimental signatures. We show that the modifications are dependent on the Rashba band index s denoting the two directions of the eigenspinors of the Rashba Hamiltonian.

The paper is organized as follows. The model Hamiltonian and the renormalizations due to s-wave interaction in the presence of SOC are discussed in Sec. II. In Sec. III, starting from the RPA self-energy of the SOC Fermi liquid, we derive all the analytical formula of the Fermi-liquid parameters in the presence of SOC. The experimental observable quantities such as the spectral function, density of states, and specific heat are calculated. Section IV is devoted to discussing the experimental measurements of these fundamental parameters and their corresponding experimental signatures. The comparisons with the ordinary Fermi liquid are also presented.

II. PERTUBATIVE THEORY OF 2D FERMI GASES WITH s-WAVE INTERACTION IN THE PRESENCE OF RASHBA SOC

A. Model Hamiltonian

We consider a 2D spin-1/2 fermionic system with Rashba-type SOC and s-wave interaction, described by the model

Hamiltonian

$$\mathcal{H} = \mathcal{H}_0 + \mathcal{H}_I. \tag{1}$$

The noninteracting part $\mathcal{H}_0$ reads as

$$\mathcal{H}_0 = \sum_{\mathbf{p}} c_{\mathbf{p}}^{\dagger}\left[\frac{\mathbf{p}^2}{2m} + \alpha\,(\hat{\mathbf{z}}\times\mathbf{p})\cdot\sigma - \mu\right]c_{\mathbf{p}}, \tag{2}$$

where $c_{\mathbf{p}} = (c_{\mathbf{p},\uparrow}, c_{\mathbf{p},\downarrow})^T$, $\mu = k_F^2/2m$ is the chemical potential, α represents the SOC strength, and k_F is the Fermi momentum in the absence of Rashba-type SOC. The reduced Plank constant $\hbar$ is taken as 1 in this paper. The noninteracting Hamiltonian $\mathcal{H}_0$ can be diagonalized in the helicity bases

$$|\mathbf{k},s\rangle = \frac{1}{\sqrt{2}}\begin{pmatrix} 1 \\ ise^{i\phi(\mathbf{k})}\end{pmatrix}, \quad s = \pm 1, \tag{3}$$

where $\phi(\mathbf{k}) = \arctan(k_y/k_x)$ and s is the helicity of the Fermi surfaces, which shows that the in-plane spin is right-handed or left-handed to the momentum. The dispersion relations for two helical branches are $\xi_{\mathbf{k},s} = (\mathbf{k}^2 + 2sk_R|\mathbf{k}| - k_F^2)/2m$, where $k_R = m\alpha$ corresponds to the recoil momentum in Refs. [5,6]. The Fermi surfaces are given by $\xi_{\mathbf{k},s} = 0$, which yields two Fermi momenta $k_s = \kappa k_F - sk_R$ with $\kappa = \sqrt{1+\gamma^2}$. We have defined the dimensionless SOC strength $\gamma = k_R/k_F$. Recently, the experimental realization of the SOC degenerated Fermi gases have been reported [5–7]. By applying a pair of laser beams to the ultracold ^{40}K or ^{6}Li atoms trapped in an anisotropic harmony trap, the equal weight combination of the Rashba-type and Dresselhaus-type SOC is generated. Their elegant experiments are performed in the weakly repulsive regime, which could provide the possibilities to study the SOC degenerated Fermi gases in the normal state.

The interacting part reads as

$$\mathcal{H}_I = 2g\int \frac{d^2\mathbf{k}d^2\mathbf{p}d^2\mathbf{q}}{(2\pi)^6} c_{\mathbf{k}+\mathbf{q},\uparrow}^{\dagger} c_{\mathbf{p}-\mathbf{q},\downarrow}^{\dagger} c_{\mathbf{p},\downarrow} c_{\mathbf{k},\uparrow}, \tag{4}$$

where $g = 2\pi N a_s/3\sqrt{2\pi}m\zeta_z$, which is controlled by the s-wave scattering length a_s. Here N is the total atom number, $\zeta_z = \sqrt{1/m\omega_z}$ is the confinement scale of the atomic cloud in the $\hat{\mathbf{z}}$ direction perpendicular to the 2D plane, and m is the mass for the ultracold atoms. Notice that the universal properties of the low-energy interaction among ultracold atoms depend only on the scattering length a_s [24–32]. We note that the gas of dimers and the repulsive Fermi gas represent two different branches of the many-body system, which both have positive values of the scattering length [33]. In this work, we focus on the normal state regime of Fermi gas in the upper branch of energy spectrum, which has been experimentally achieved by ramping up adiabatically the value of the scattering length, starting from the value $a_s = 0$ [34].

B. Renormalizations due to the s-wave interaction

Let's consider the problem in the helicity bases $|\mathbf{k},s\rangle$. The noninteracting Green's function is

$$G_s^0(\mathbf{k},\omega) = \frac{1}{\omega - \xi_{\mathbf{k},s} + i\,\mathrm{sgn}(\omega)0^+}. \tag{5}$$

The Dyson's equation expresses the relation between the noninteracting and interacting Green's functions in terms of the self-energy Σ_s as

$$G_s(\mathbf{k},\omega) = \frac{1}{\omega - \xi_{\mathbf{k},s} - \Sigma_s(\mathbf{k},\omega)}. \tag{6}$$

All the many-body physics is contained in the self-energy Σ_s. The poles of interacting Green's function $G_s(\mathbf{k},\omega)$ give the quasiparticle excitations, of which lifetime $\tau_s = 1/\Gamma_s$ can be obtained from the imaginary part of self-energy as

$$\Gamma_s(\mathbf{k}) = -2\mathrm{Im}\Sigma_s(\mathbf{k},\xi_{\mathbf{k},s}). \tag{7}$$

The real part of the self-energy gives a modification of dispersion relations. At low temperature, the properties of the low-energy excitation in the vicinity of the Fermi surface is essential. Thus we can expand the real part of the self-energy to the first order of ω and $|\mathbf{k}| - k_s$ as

$$\begin{aligned}\mathrm{Re}\Sigma_s(\mathbf{k},\omega) = {}& \mathrm{Re}\Sigma_s(\mathbf{k}_s,0) + \omega\partial_\omega \mathrm{Re}\Sigma_s(\mathbf{k}_s,\omega)|_0 \\ & + (\mathbf{k}-\mathbf{k}_s)\cdot\nabla_{\mathbf{k}}\mathrm{Re}\Sigma_s(\mathbf{k},0)|_{\mathbf{k}_s}.\end{aligned} \tag{8}$$

The interacting Green's function now becomes

$$G_s(\mathbf{k},\omega) = \frac{Z_s}{\omega - \xi_{\mathbf{k},s}^* + i(1/2)\Gamma_s(\mathbf{k})}, \tag{9}$$

where $\xi_{\mathbf{k},s}^*$ is the modified energy dispersion. The Green's function acquires a renormalized factor,

$$Z_s = \frac{1}{1 - A_s}, \tag{10}$$

where $A_s = \partial_\omega \mathrm{Re}\Sigma_s(\mathbf{k}_s,\omega)|_0$. The Fermi velocity $v_{k_s} = \partial\xi_{\mathbf{k},s}^*/\partial k|_{k_s}$ can be calculated as follows:

$$\left.\frac{\partial\xi_{\mathbf{k},s}^*}{\partial k}\right|_{|\mathbf{k}|=k_s} = Z_s[\kappa k_F/m + \partial_k \mathrm{Re}\Sigma_s(\mathbf{k},0)|_{k_s}]. \tag{11}$$

For noninteracting Fermi gas, the Fermi velocity is $v_{k_s}^0 = \kappa k_F/m$. Therefore we introduce the effective mass via $\partial\xi_{\mathbf{k},s}^*/\partial k|_{|\mathbf{k}|=k_s} = \kappa k_F/m_s^*$. The effective mass in terms of self-energy is

$$\frac{m_s^*}{m} = \frac{1}{Z_s}\left(1 + \frac{m}{\kappa k_F}\partial_k \mathrm{Re}\Sigma_s^R(\mathbf{k}_s,0)\right)^{-1}. \tag{12}$$

Equations (7), (10), and (12) are our starting points of microscopic calculations of normal-state properties, which embody the main properties of a quasiparticle in the Landau theory of Fermi liquids.

III. SOC FERMI-LIQUID PARAMETERS WITH REPULSIVE s-WAVE INTERACTION

A. RPA self-energy

To investigate the renormalization effects in two Rashba energy bands separately, it is convenient to work in the helicity bases. The interacting part of the Hamiltonian in the helicity bases is rewritten as

$$\mathcal{H}_I = \sum_{\mathbf{k},\mathbf{p},\mathbf{q}} V_{ss';rr'}(\mathbf{k},\mathbf{p},\mathbf{q})\varphi_{\mathbf{k}+\mathbf{q},s'}^{\dagger}\varphi_{\mathbf{p}-\mathbf{q},r'}^{\dagger}\varphi_{\mathbf{p},r}\varphi_{\mathbf{k},s}, \tag{13}$$

where the interaction vertex $V_{ss';rr'}(\mathbf{k},\mathbf{p},\mathbf{q}) = g f_{ss'}(\theta_{\mathbf{k}},\theta_{\mathbf{k}+\mathbf{q}})$ $f_{rr'}(\theta_{\mathbf{p}},\theta_{\mathbf{p}-\mathbf{q}})$. Due to the presence of SOC, the spin is locked to

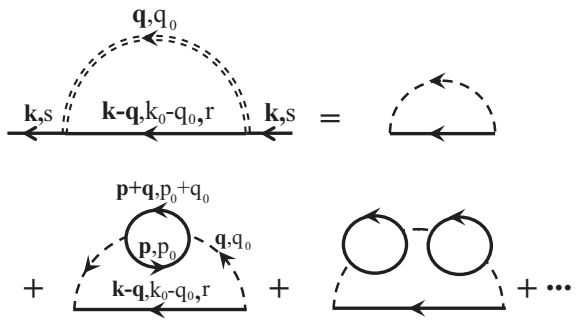

FIG. 1. Feynman diagrams for the self-energy of the SOC Fermi liquid in the presence of s-wave interaction. The Feynman rules are defined under the helicity bases. The labels s and r denote the helicity index. The self-energy is calculated within the framework of the RPA [35].

momentum. The interaction vertex acquires an overlap factor $f_{ss'}(\theta_{\mathbf{k}},\theta_{\mathbf{k}+\mathbf{q}})$, and $f_{rr'}(\theta_{\mathbf{p}},\theta_{\mathbf{p}-\mathbf{q}})$, which is defined by

$$f_{ss'}(\theta_{\mathbf{k}},\theta_{\mathbf{p}}) = \tfrac{1}{2}(1+ss'e^{i[\theta_{\mathbf{k}}-\theta_{\mathbf{p}}]}), \tag{14}$$

where $\theta_{\mathbf{k}}$ and $\theta_{\mathbf{p}}$ are the azimuthal angles of $\mathbf{k}$ and $\mathbf{p}$, respectively. Within the framework of the RPA, the interaction vertex is modified as (see Fig. 1)

$$V^{\mathrm{RPA}}_{ss',rr'}(\mathbf{k},\mathbf{p},\mathbf{q},\omega) = \frac{g}{\epsilon(\mathbf{q},\omega)} f_{ss'}(\theta_{\mathbf{k}},\theta_{\mathbf{k}+\mathbf{q}}) f_{rr'}(\theta_{\mathbf{p}},\theta_{\mathbf{p}-\mathbf{q}}), \tag{15}$$

where the dielectric function $\epsilon(\mathbf{q},\omega) = 1 + g\chi(\mathbf{q},\omega)$ and $\chi(\mathbf{q},\omega)$ is the bare density-density susceptibility of noninteracting SOC Fermi gas. In the long-wavelength and low-frequency limit, the susceptibility can be carried out as

$$\begin{aligned} \mathrm{Re}\chi(y) &= \frac{m}{\pi}\left[1 - \frac{|y|}{\sqrt{y^2-1}}\Theta(|y|-1)\right], \\ \mathrm{Im}\chi(y) &= \frac{m}{\pi}\frac{y}{\sqrt{1-y^2}}\Theta(1-|y|), \end{aligned} \tag{16}$$

where $y = m\omega/\kappa k_F|\mathbf{q}|$. It can be seen from Eq. (16) that the susceptibility satisfies the following relations:

$$\chi^*(\mathbf{q},\omega) = \chi(-\mathbf{q},-\omega) = \chi(\mathbf{q},-\omega). \tag{17}$$

It is important to notice that the bare susceptibility is real for $|\omega| > v_F\sqrt{1+\gamma^2}|\mathbf{q}|$. For $|\omega| < v_F\sqrt{1+\gamma^2}|\mathbf{q}|$, the bare susceptibility in Eq. (16) contains an imaginary part which represents the absorptive behavior of the medium. This imaginary part is responsible for the finite lifetime of the quasiparticle in the medium. Along the imaginary axis, the analytical formula of $\chi(\mathbf{q},\omega)$ is much simpler (see Fig. 2):

$$\chi(\mathbf{q},i\omega) = \frac{m}{\pi}\left[1 - \frac{|y|}{\sqrt{y^2+1}}\right]. \tag{18}$$

The RPA self-energy (see Fig. 1) is

$$\Sigma_s(\mathbf{k},\omega) = i\int_C \frac{d^2\mathbf{q}dq_0}{(2\pi)^3}\sum_r \frac{g\mathcal{F}_{sr}}{\epsilon(\mathbf{q},q_0)} G^0_r(\mathbf{k}-\mathbf{q},\omega-q_0), \tag{19}$$

where the $\mathcal{F}_{sr}$ is the overlap factor:

$$\mathcal{F}_{sr} = \frac{1+sr\cos(\theta_{\mathbf{k}}-\theta_{\mathbf{k}-\mathbf{q}})}{2}. \tag{20}$$

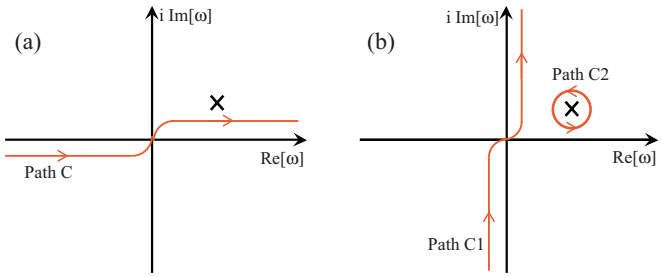

FIG. 2. (Color online) (a) The contours of integration in the complex ω plane for the self-energy given by Eq. (19). For intermediate states with the energy $0 < \xi_{\mathbf{k}-\mathbf{q},r} < \omega$, the pole of the propagator falls in the first quadrant. (b) Schematic of the deformation of the contour into the imaginary axis. The self-energy given by Eq. (19) is equal to the integration along the path $C1$ with an additional contribution of the residue as shown by the integral path $C2$.

The integral path C is shown in Fig. 2(a). After deformation of the contour path in Fig. 2(b), the pole gives rise to a residue contribution,

$$\Sigma^{\mathrm{pole}}_s(\mathbf{k},\omega) = -\sum_r \int_{D_r} \frac{d^2\mathbf{q}}{(2\pi)^2}\frac{g}{\epsilon}\mathcal{F}_{sr}, \tag{21}$$

where the region of integration D_r is $k_r < |\mathbf{k}-\mathbf{q}| < |\mathbf{k}| - (r-s)k_R$ and $\epsilon = 1 + g\chi_0(\mathbf{q},\omega-\xi_{\mathbf{k}-\mathbf{q},r})$. The line integral along the imaginary axis is

$$\Sigma^{\mathrm{line}}_s(\mathbf{k},\omega) = -\int_{-\infty}^{\infty}\frac{d^2\mathbf{q}dq_0}{(2\pi)^3}\sum_r \frac{g\mathcal{F}_{sr}}{\epsilon(\mathbf{q},iq_0)}\frac{1}{\omega - iq_0 - \xi_{\mathbf{k}-\mathbf{q}r}}. \tag{22}$$

The total self-energy is given by

$$\Sigma_s = \Sigma^{\mathrm{pole}}_s + \Sigma^{\mathrm{line}}_s. \tag{23}$$

The advantage of this decomposition is that the imaginary part is given by the contribution of residue, and the real part is mainly determined by the line integral.

B. Quasiparticle lifetime

The quasiparticle lifetime can be calculated by the imaginary part of the self-energy, which comes from the contribution of residue in Eq. (21). At zero temperature and for quasiparticle $\xi_{\mathbf{k},s} > 0$, the imaginary part of the self-energy reads as

$$\begin{aligned} \Gamma_s(\mathbf{k}) = 2\sum_{\mathbf{q},r}&\Theta(\xi_{\mathbf{k}-\mathbf{q},r})\Theta(\xi_{\mathbf{k},s}-\xi_{\mathbf{k}-\mathbf{q},r}) \\ &\times \mathrm{Im}V^{\mathrm{RPA}}_{sr;sr}(\mathbf{k},\mathbf{k}-\mathbf{q},\mathbf{q};\xi_{\mathbf{k},s}-\xi_{\mathbf{k}-\mathbf{q},r}). \end{aligned} \tag{24}$$

The imaginary part of the RPA vertex in the helicity bases is

$$\mathrm{Im}V^{\mathrm{RPA}}_{sr;rs}(\mathbf{k},\mathbf{k}-\mathbf{q},\mathbf{q},\mathbf{k};w) = g\mathcal{F}_{sr}\mathrm{Im}\frac{1}{\epsilon(y)}, \tag{25}$$

where $w = \xi_{\mathbf{k},s} - \xi_{\mathbf{k}-\mathbf{q},r}$ and $y = w/v_F|\mathbf{q}|$. Since the main contribution of the integral comes from the forward scattering, i.e., $y \ll 1$, the density-density susceptibility can be expanded about $y = 0$. One finds that the susceptibility in this neighborhood is

$$\chi(y) = \frac{m}{\pi}(1+iy) + O(y^2). \tag{26}$$

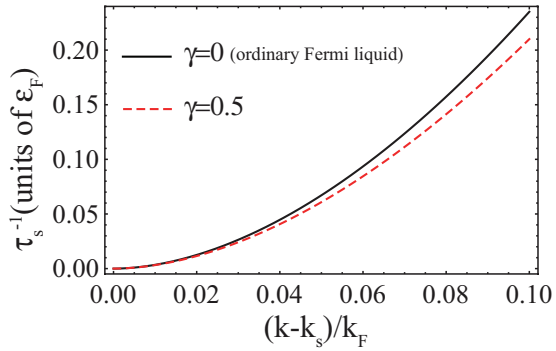

FIG. 3. (Color online) The inverse of the lifetime τ_s for ^{40}K ultracold atoms as a function of the momentum k in the vicinity of the Fermi surface. The lifetime of the quasiparticle is enhanced due to the presence of SOC. The parameters taken here are as follows: the number of atoms is about 10^4, $k_R = h/\lambda$ with $\lambda = 773$ nm, $\gamma = 0.5$, trap frequency $\omega_z = 2\pi \times 400$ Hz, and $a_s = 32a_0$, where a_0 is the Bohr radius. The unit $\epsilon_F = \hbar \times 0.21$ MHz.

The imaginary part of the RPA vertex becomes

$$\mathrm{Im}V^{\mathrm{RPA}}_{sr;rs}(\mathbf{k},\mathbf{k}-\mathbf{q},\mathbf{q};w) \simeq -\frac{m^2g^2}{(mg+\pi)^2}\frac{\pi}{m}y\mathcal{F}_{sr}. \tag{27}$$

Substituting Eq. (27) into Eq. (24), the inverse lifetime $\Gamma_s(k)$ can be evaluated as

$$\Gamma_s(\mathbf{k}) = -\frac{m^2g^2\epsilon_F}{\pi(mg+\pi)^2}\delta^2\left\{\ln\frac{\delta}{8}-\frac{1}{2}-\gamma^2\ln\frac{\gamma}{4}\right\}, \tag{28}$$

where $\delta = (k-k_s)/k_F$. The result for ordinary Fermi liquid in the presence of s-wave repulsive interaction can be obtained by taking the limit $\gamma \to 0$ in Eq. (28). The effect of SOC is shown in Fig. 3 via the comparison with the ordinary Fermi liquid with the same strength of s-wave repulsive interaction, from which we can conclude that the quasiparticle is much stabler in the presence of SOC.

C. Green's function renormalization factor

Our starting point is the real part of the self-energy which contains two parts: one is the residue contribution given by Eq. (21); the other is the integral along the imaginary axis given by Eq. (22). Thus we want to evaluate

$$A_s = A_s^{\mathrm{pole}} + A_s^{\mathrm{line}} = \partial_\xi \Sigma_s^{\mathrm{pole}}(\mathbf{k}_s,\xi)|_{\xi=0} + \partial_\xi \Sigma_s^{\mathrm{line}}(\mathbf{k}_s,\xi)|_{\xi=0}. \tag{29}$$

Given the rotation symmetry, we only need to consider $\mathbf{k}_s = k_s\mathbf{e}_x$. The first term in Eq. (29) is

$$A_s^{\mathrm{pole}} = \sum_r \int \frac{d^2\mathbf{q}}{(2\pi)^2}\delta(\xi_{\mathbf{k}_s-\mathbf{q},r})\frac{g}{\epsilon}\mathcal{F}_{sr}. \tag{30}$$

The second term in Eq. (29) can be integrated by parts, which gives two parts: the first one reads as

$$A_s^{\mathrm{line}} = -\sum_r \int \frac{d^2\mathbf{q}}{(2\pi)^2}\delta(\xi_{\mathbf{k}_s-\mathbf{q},r})\frac{g}{\epsilon}\mathcal{F}_{sr}, \tag{31}$$

which cancels the residue contribution given by Eq. (30). Thus the final result of Eq. (29) can be expressed as

$$A_s = -\frac{mgk_F^2}{(2\pi)^3k_s^2}\int_0^{2\pi}d\phi\int_0^{\infty}d\bar{y}\int_0^{\infty}dx\sum_r \mathrm{Im}f_{sr}(x,\bar{y},\phi), \tag{32}$$

where we have defined $\bar{y} = mw/qk_s$, $x = q/2k_s$, and

$$f_{sr}(x,\bar{y},\phi) = \frac{\mathcal{F}_{sr}}{i\bar{y}-\mu(x,\phi)}\frac{1}{\epsilon^2}\frac{\partial\epsilon}{\partial\bar{y}}. \tag{33}$$

Here $\mu_{s,r}(x,\phi) = m\xi_{\mathbf{k}-\mathbf{q},r}/|\mathbf{q}|k_s$, and the overlap factor $\mathcal{F}_{sr}(x,\phi) = 1/2 + sr(1-2x\cos\phi)/2l$, with $l = |\mathbf{k}-\mathbf{q}|/k_s = \sqrt{1-4x\cos\phi+4x^2}$.

From Eqs. (10), (32), and (33), we can obtain the renormalization factor straightforwardly:

$$Z_s^{-1} = 1 + \frac{m^2g^2}{8\pi(mg+\pi)}\frac{1}{(\kappa-s\gamma)^2} = 1 + \frac{m^2g^2}{8\pi(mg+\pi)}[1+s\gamma+O(\gamma^2)]. \tag{34}$$

The renormalization factor turns out to be dependent on the helicity s and the leading correction due to SOC is $O(\gamma)$, which is different from the results of 2D electron gas (2DEG) with SOC in semiconductors [36]. We show the analytical results along with the numerical calculation for Z_s as a function of the s-wave scattering length in Fig. 4 and the strength of SOC in Fig. 5. The Green's function renormalization factor for ordinary Fermi liquid is also shown for comparison in Fig. 4. We can see from Fig. 5 that the renormalization factor is reduced for the $s = +1$ branch and enhanced for the $s = -1$ branch with increasing strength of SOC.

D. Effective mass

The effective mass can be evaluated by the real part of the static self-energy in the vicinity of the Fermi surface from Eq. (12). In contrast to the calculation of the renormalization factor Z_s, the contribution of residue is irrelevant now. The correction of the effective mass is isotropic due to the rotation

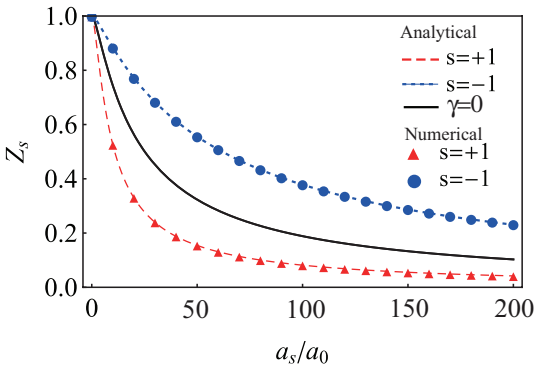

FIG. 4. (Color online) Renormalization factor Z_s as a function of scattering length a_s with the same parameters as in Fig. 3. The black thick line represents the renormalization factor of ordinary Fermi gases ($\gamma = 0$). The red (dashed) and blue (dotted) lines represent the analytical results for the SOC Fermi gas given by Eq. (34). The discrete points are evaluated numerically.

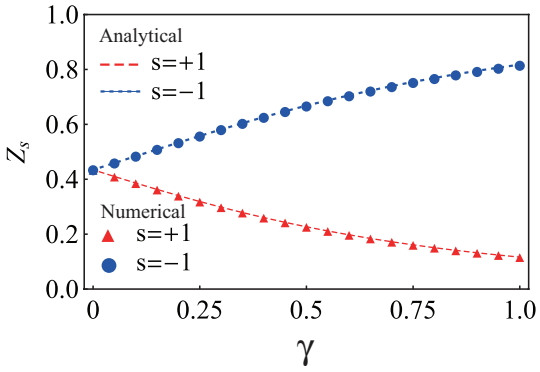

FIG. 5. (Color online) Renormalization factor Z_s as a function of dimensionless SOC strength γ with the same parameters as in Fig. 3. The red (dashed) and blue (dotted) lines represent the analytical results for the SOC Fermi gas given by Eq. (34). The discrete points are evaluated numerically.

symmetry. Without loss of generalities, we assume $\mathbf{k}_s = k_s \mathbf{e}_x$ in the following. We begin with

$$\partial_k \mathrm{Re}\Sigma_s(\mathbf{k},0)|_{|\mathbf{k}|=k_s} = \mathrm{Re}\int_{-\infty}^{\infty} \frac{d^2\mathbf{q}dw}{(2\pi)^3}\partial_k \sum_r \frac{1}{iw+\xi_{\mathbf{k}-\mathbf{q},r}} V^{\mathrm{RPA}}_{sr;sr}(\mathbf{k},\mathbf{q},iw). \quad (35)$$

The interaction vertex is dependent on the external momentum $\mathbf{k}$ because of the overlap of the helical eigenstates. It is instructive to consider some special cases. For weak SOC ($\gamma \ll 1$), the integration in Eq. (35) can be expanded to

$$\partial_k \mathrm{Re}\Sigma_s(\mathbf{k},0)|_{|\mathbf{k}|=k_s} = \frac{k_F g}{4\pi} s\gamma + O(\gamma^2). \quad (36)$$

In contrast to the SOC Fermi liquid with Coulomb interaction [36], our result is band dependent and has a first-order correction γ. The effective mass reads as

$$\frac{m_s^*}{m} = Z_s^{-1}\left(1 + s\frac{mg}{mg+\pi}\frac{\gamma}{4\kappa}\right)^{-1}. \quad (37)$$

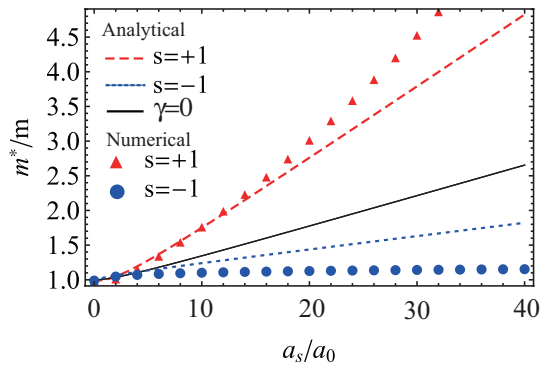

FIG. 6. (Color online) Effective mass as a function of s-wave scattering length a_s with the same parameters as in Fig. 3. The red (dashed) and blue (dotted) lines denote the case for $s = +1$ and $s = -1$, respectively. The solid triangle and circle points are the corresponding numerical results. The black line represents the analytical results for ordinary Fermi liquid ($\gamma = 0$). The many-body modifications of the effective mass are dependent on the helical bands.

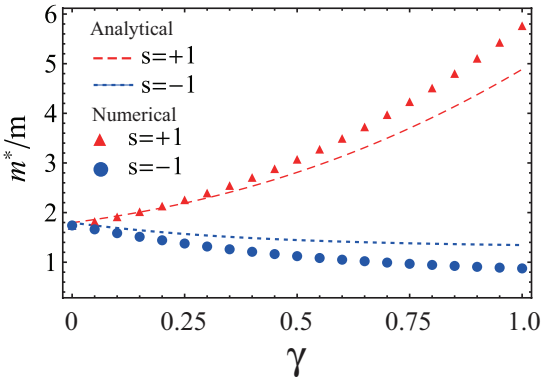

FIG. 7. (Color online) Effective mass as a function of the strength of SOC γ with the same parameters as in Fig. 3. The red (dashed) and blue (dotted) lines denote the case for $s = +1$ and $s = -1$, respectively. The solid triangle and circle points are the corresponding numerical results.

For strong SOC ($\gamma \sim 1$), we show the numerical results along with the analytical results of Eq. (37) in Fig. 6. The effect of SOC is shown in Fig. 7, from which we can see that the effective mass for the $s = +1$ branch is enhanced while that for the $s = -1$ branch is reduced with increasing strength of SOC.

E. Spectral function, density of state, and specific heat

A close related quantity is the spectral function $A(\mathbf{k},\omega)$, which is the imaginary part of the single-particle Green's function [37,38]

$$A(\mathbf{k},\omega) = -\frac{1}{\pi}\mathrm{Im}G^{\mathrm{ret}}(\mathbf{k},\omega), \quad (38)$$

where $G^{\mathrm{ret}}(\mathbf{k},\omega)$ is the retarded Green's function. It can be straightforwardly evaluated from the time-ordered Green's function $G(\mathbf{k},\omega)$ as

$$\begin{aligned} \mathrm{Im}G^{\mathrm{ret}}(\mathbf{k},\omega) &= \mathrm{Im}G(\mathbf{k},\omega)\mathrm{sign}(\omega), \\ \mathrm{Re}G^{\mathrm{ret}}(\mathbf{k},\omega) &= \mathrm{Re}G(\mathbf{k},\omega). \end{aligned} \quad (39)$$

With the great improvements in the spectroscopic technique, it has been possible to directly measure the low-energy spectral weight function of a 2D system in the momentum-resolved radio frequency (rf) experiments [39–41]. In Fig. 8, we show the spectral functions of the two Rashba bands separately. The spectral functions at the Fermi surfaces as shown in Figs. 8(a) and 8(b) (vertical arrow) have the form

$$A(\mathbf{k}_s,\omega) = Z_s\delta(\omega). \quad (40)$$

Figures 8(c) and 8(d) are density plots of the spectral functions, which could be compared with the results of the momentum-resolved rf spectroscopy in current experiments.

Given the spectral functions, we can obtain the density of states (DOS) of the fermionic system with SOC via [37,38]

$$\rho(\omega) = \sum_s \rho_s(\omega) = \sum_s \int \frac{d^2\mathbf{k}}{(2\pi)^2} A_s(\mathbf{k},\omega). \quad (41)$$

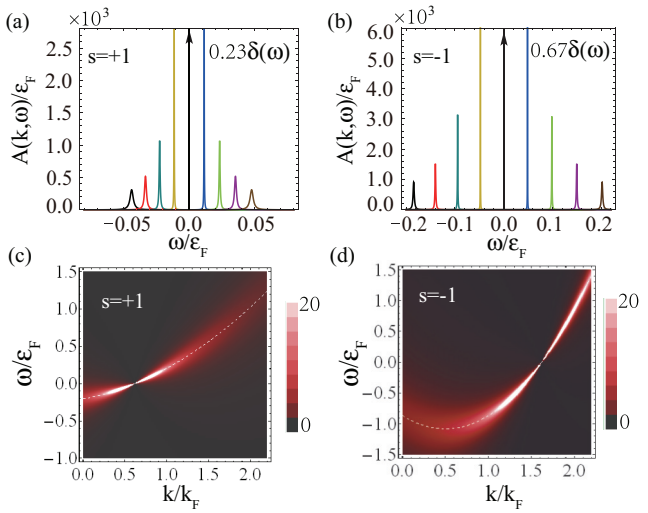

FIG. 8. (Color online) Zero temperature spectral function at different values of $(k-k_s)/k_F$ are shown in panels (a) and (b). All the parameters are the same as in Fig. 3. (a) $s=+1$; (b) $s=-1$. The eight peaks, from left to right, correspond to $(k-k_s)/k_F=-0.01$, -0.075, -0.05, -0.025, 0.025, 0.05, 0.075, and 0.01. The vertical arrows in panels (a) and (b) denote δ functions at $\omega=0$ with weights of 0.23 and 0.67, respectively. Panels (c) and (d) are density plots of the spectral functions for the same parameters as above, which correspond to $s=+1$ and $s=-1$, respectively. The white dashed line denotes the modified single-particle dispersion.

For the noninteracting case, the DOS now becomes

$$\rho^0(\omega)=\begin{cases}0, & \omega<-\frac{\kappa^2k_F^2}{2m},\\ \frac{m}{\pi}\frac{\gamma}{\sqrt{2m\omega/k_F^2+\kappa^2}}, & -\frac{\kappa^2k_F^2}{2m}<\omega<-\frac{k_F^2}{2m},\\ \frac{m}{\pi}, & \omega>-\frac{k_F^2}{2m}.\end{cases}\tag{42}$$

The DOS is modified in the presence of s-wave interaction. On the Fermi surfaces, for noninteracting SOC Fermi gas, the DOS in units of m/π is given by $\rho^0_{+1}(E_F)=0.28$, $\rho^0_{-1}(E_F)=0.72$, and $\rho^0(E_F)=1$ for $\gamma=0.5$. For the interacting SOC Fermi gas, the DOS is evaluated numerically as follows: $\rho_{+1}(E_F)=1.37$, $\rho_{-1}(E_F)=0.83$, and $\rho(E_F)=2.20$, where all the parameters are the same as in Fig. 3.

The quasiparticles from two helical bands contribute to the specific heat. At low temperature, the specific heat is proportional to the DOS on the Fermi surfaces and the temperature T. Thus the ratio between the specific heats at low temperature is

$$\frac{c_v}{c_v^0}=\frac{\rho(E_F)}{\rho^0(E_F)}=2.20,\tag{43}$$

where c_v^0 is the specific heat of SOC Fermi gases without interactions.

IV. DISCUSSIONS AND SUMMARIES

We have obtained various normal-state quantities of 2D SOC Fermi gases in the presence of repulsive s-wave interaction. Ultimately, to make contact with experiments, two practical considerations warrant mention. (i) The repulsive s-wave interaction can be achieved on the upper branch of a Feshbach resonance. One problem that should be considered is that the upper branch of a Feshbach resonance is an excited branch and will decay to the BEC molecule state due to inelastic three-body collisions [42]. However, with small scattering length, the decay rate is well suppressed [1,43] and the system may be metastable for observation. (ii) Recently, the SOC degenerate Fermi gases have been realized in the ultracold atom systems [5,6]. The effective SOC generated in their experimental schemes is an equal weight combination of Rashba-type and Dresselhaus-type SOC. In this paper, we investigate the case of Rashba-type SOC. The Dresselhaus-type SOC is presented in Appendix A and is shown to give the same normal-state properties as the Rashba case.

In the current experiments, we consider the following typical experimental parameters for quasi-2D systems. One can trap about 10^4 ^{40}K atoms within a pancake-shaped harmonic potential with the trap frequency chosen as $2\pi\times(10,10,400)$ Hz along the $(\hat{x},\hat{y},\hat{z})$ directions. The system size can be estimated as (37.8, 37.8, 5.98) μm. The other related parameters are taken as $a_s=32a_0$, $\gamma=0.5$, and $k_R=2\pi/\lambda=8.128\times10^6$ m. The Fermi-liquid parameters are listed in Table I under this typical experimental setup. For comparison, we give the results of ordinary Fermi liquid and the 2DEG in semiconductors together. Note that the single-particle spectral function captures the valuable information for low-energy excitations of the Fermi liquid and can be measured by means of momentum-resolved rf experiments [39–41,44]. The rf spectroscopy is a technique used to probe atomic correlation by exciting atoms from occupied hyperfine states to another (usually empty) reference hyperfine state. The single-particle spectral function is obtained in experiment through the momentum-resolved rf-transfer strength. As a result, the inferences drawn from the spectral function in the vicinity of the Fermi surfaces can be used to determine the Fermi-liquid parameters describing the low-energy behaviors of the normal state. Up to now, the rf experiment is the most promising method in ultracold atomic gases to measure these Fermi-liquid parameters.

TABLE I. Normal-state properties for SOC Fermi liquid ($\gamma=0.5$), ordinary Fermi liquid ($\gamma=0$), and 2DEG ($\gamma=0.051$) in semiconductor. All other parameters used here are the same as in Fig. 3.

	$\gamma=0.5$	$\gamma=0$	2DEG ($\gamma=0.051$)[a]
$1/\tau_s$[b]	0.73 kHz	0.67 kHz	55.36 GHz
Z_s	$Z_{+1}=0.23$ $Z_{-1}=0.67$	0.96	0.97
m_s^*/m	$m^*_{+1}/m=4.88$ $m^*_{-1}/m=1.16$	1.04	0.98

[a]The results for 2DEG in InGaAs are taken from Ref. [36]. Compared with the SOC Fermi liquid in the presence of s-wave interaction, the results for the 2DEG with Coulomb interaction are independent on the energy band, and the leading order correction relative to the SOC strength is γ^2.

[b]The values of the inverse lifetime are evaluated at $(k-k_{\pm1})/k_F=0.01$. Compared with 2DEG in the typical semiconductor, the quasiparticle in ultracold atomic gases is much stabler.

In summary, we studied the normal-state properties of the SOC Fermi gas with repulsive s-wave interaction. The quasiparticle lifetime τ_s, the renormalization factor Z_s, and the effective mass m_s^*/m, which embody the main properties of a quasiparticle, have been calculated. To make contact with the experiments directly, we calculated the spectral function $A(\mathbf{k},\omega)$, the density of state $\rho(\omega)$, and the specific heat c_v at low temperature. These quantities provide a good description of the low-energy physics with SOC and s-wave interaction, which are measurable in current experiments. The analytical and numerical results show that the normal-state properties are distinct for the two energy bands, and the leading correction relative to the ordinary Fermi liquid with s-wave interaction is on the order of γ, which is strikingly different from the SOC Fermi liquid with Coulomb interaction [36]. We expect our microscopic calculations of the Fermi-liquid parameters and related quantities would have immediate applicability to the SOC Fermi gases in the upper branch of the energy spectrum.

ACKNOWLEDGMENTS

We acknowledge helpful discussions with Jinwu Ye, Han Pu, Congjun Wu, and Hui Hu. This work was supported by the NKBRSFC under Grants No. 2009CB930701, No. 2010CB922904, No. 2011CB921502, and No. 2012CB821300, the NSFC under Grant No. 10934010, and the NSFC-RGC under Grants No. 11061160490 and No. 1386-N-HKU748/10.

APPENDIX A : RELATIONSHIPS BETWEEN THE RASHBA SOC AND DRESSELHAUS SOC

In this paper, the normal-state properties of the Fermi liquid with Rashba-type SOC are studied. Now, we would like to demonstrate that another type of SOC, namely, the Dresselhaus-type, gives exactly the same results for the normal-state properties considered here.

We start with the single-particle Hamiltonian with Dresselhaus SOC [7]:

$$\mathcal{H}_D = \frac{\mathbf{p}^2}{2m} + \alpha(-p_y\sigma_x - p_x\sigma_y) - \mu. \tag{A1}$$

The helicity bases with Dresselhaus SOC are

$$|\mathbf{p},s\rangle_D = -\frac{1}{\sqrt{2}}\begin{pmatrix} 1 \\ ise^{-i\phi(\mathbf{p})} \end{pmatrix}, \quad s = \pm 1, \tag{A2}$$

where the subscript D represents the Dresselhaus-type SOC. The starting point of the microscopic calculation is the self-energy Σ_s for each band. To illustrate the relationships of the two types of SOC, it is essential to derive the relationships of the Feynman rules between the two cases. For the Dresselhaus-type SOC, the noninteracting Green's function and the interaction vertex in the helicity bases read as

$$G_s^D(\mathbf{k},\omega) = \frac{1}{\omega - \xi_{\mathbf{k},s} + i\,\mathrm{sgn}(\omega)0^+}, \tag{A3}$$

$$V^D_{ss';rr'}(\mathbf{k},\mathbf{p},\mathbf{q}) = g f^D_{ss'}(\theta_{\mathbf{k}},\theta_{\mathbf{k}+\mathbf{q}}) f^D_{rr'}(\theta_{\mathbf{p}},\theta_{\mathbf{p}-\mathbf{q}}). \tag{A4}$$

The energy spectrum of the Dresselhaus-type SOC is the same as that of the Rashba-type SOC. Thus the single-particle retarded Green's function within the Dresselhaus representation is the same as the result for the Rashba-type SOC given in Eq. (5). The overlap factor $f^D_{ss'}(\theta_{\mathbf{k}},\theta_{\mathbf{k}+\mathbf{q}})$ for the Dresselhaus-type SOC is given by

$$f^D_{ss'}(\theta_{\mathbf{k}},\theta_{\mathbf{k}+\mathbf{q}}) = \tfrac{1}{2}(1 + ss'e^{-i[\phi(\mathbf{k})-\phi(\mathbf{k}+\mathbf{q})]}). \tag{A5}$$

Compared with Eq. (14), we find the overlap factors are conjugated for the two cases:

$$f^D_{ss'}(\theta_{\mathbf{k}},\theta_{\mathbf{k}+\mathbf{q}}) = f^R_{ss'}(\theta_{\mathbf{k}},\theta_{\mathbf{k}+\mathbf{q}})^*. \tag{A6}$$

The bare susceptibility in the Matsubara formalism is given by

$$\chi^D(\mathbf{q},i\omega_n) = k_B T \sum_{\substack{\mathbf{k},i\omega_m \\ s,r}} G_s^D(\mathbf{k},i\omega_m) G_r^D(\mathbf{k}-\mathbf{q},i\omega_m - i\omega_n)\mathcal{F}^D_{sr}, \tag{A7}$$

where the factor

$$\mathcal{F}^D_{sr} = \frac{1 + sr\cos\theta}{2} \tag{A8}$$

is the same as that of the Rashba case in Eq. (20). So the bare susceptibility χ^D for the Dresselhaus-type SOC is equal to that of the Rashba-type SOC. The self-energy is given by Eqs. (21) and (22). The integrand function includes the following factors: the single-particle Green's function, the bare susceptibility $\chi^D(\mathbf{q},i\omega_n)$, and the overlap factor $\mathcal{F}^D_{sr}$, which are all demonstrated to be the same for the two types of SOC. Therefore we conclude that the normal-state properties calculated here, such as the quasiparticle lifetime $\tau_s(\mathbf{k})$, the renormalization factor Z_s, and the effective mass m_s^*/m are all exactly the same for the two types of SOC.

APPENDIX B : SPECTRAL FUNCTION IN THE SPIN REPRESENTATION

In this work, we studied the Fermi-liquid parameters such as $\tau_{\mathbf{k},s}$, Z_s, and m_s^*/m and associated experimental observables such as $A_s(\mathbf{k},\omega)$, $\rho(E_F)$, and c_v in the helicity representation. Theoretically speaking, the helicity representation provides a clear description of the microscopic picture of the single-particle excitation of the repulsive SOC Fermi gas. In the normal-state regime, the quasiparticle of repulsive SOC Fermi gas can be adiabatically connected with the particle of the same helicity in the noninteracting theory. In this Appendix, we also present the main results in the spin representation, since experimentalists find it handier to work with spin representation. In the following, we derive the corresponding transformations between these two representations.

In the spin representation, the Green's function of the SOC Fermi gas is also a 2×2 matrix. The noninteracting Green's function is given by

$$G_0(\mathbf{k},\omega)_{\alpha,\beta} = \sum_s \frac{1}{\omega - \xi_{\mathbf{k},s} + i\,\mathrm{sgn}(\omega)0^+} P_s(\mathbf{k}), \tag{B1}$$

where $P_s(\mathbf{k}) = [1 + s(\hat{\mathbf{z}} \times \hat{\mathbf{k}}) \cdot \boldsymbol{\sigma}]/2$ is the projection operator to the helicity representation. Considering the s-wave interaction, there are modifications of the quasiparticle dispersion $\xi^*_{\mathbf{k},s}$ and a finite lifetime of the quasiparticle $\tau_{\mathbf{k},s}$ corresponding

to the imaginary part of the self-energy, such as

$$G_{\alpha,\beta}(\mathbf{k},\omega)=\sum_{s}\frac{1}{\omega-\xi^{*}_{\mathbf{k},s}-i\mathrm{sgn}(\omega)\frac{\tau_{\mathbf{k},s}}{2}}P_{s}(\mathbf{k}). \quad \text{(B2)}$$

Where α and β are spin indexes and s is a helicity index. Then we can obtain the spectral function in the spin s_z representation as

$$A_{\alpha,\beta}(\mathbf{k},\omega)=\sum_{s}P_{s}(\mathbf{k})_{\alpha,\beta}A_{s}(\mathbf{k},\omega). \quad \text{(B3)}$$

More specifically, we have

$$A_{\uparrow,\uparrow}(\mathbf{k},\omega)=A_{\downarrow,\downarrow}(\mathbf{k},\omega)=\tfrac{1}{2}[A_{+}(\mathbf{k},\omega)+A_{-}(\mathbf{k},\omega)], \quad \text{(B4)}$$

$$A_{\uparrow,\downarrow}(\mathbf{k},\omega)=A_{\downarrow,\uparrow}(\mathbf{k},\omega)^{*}=-\frac{ie^{-i\theta_{\mathbf{k}}}}{2}[A_{+}(\mathbf{k},\omega)-A_{-}(\mathbf{k},\omega)]. \quad \text{(B5)}$$

The elements $A_{\uparrow,\uparrow}$ and $A_{\downarrow,\downarrow}$ are real and equal to each other, while the off-diagonal elements $A_{\uparrow,\downarrow}$ and $A_{\uparrow,\downarrow}$ have an angle dependence, which is the very effect of SOC.

In addition, the other quantities, such as the density of states at the Fermi energy and the low-temperature specific heat, are all independent of the representation. Therefore they could be compared with experiment straightforwardly without further transformations.

[1] G. B. Jo, Y. R. Lee, J. H. Choi, C. A. Christensen, T. H. Kim, J. H. Thywissen, D. E. Pritchard, and W. Ketterle, Science **325**, 1521 (2009).
[2] V. B. Shenoy and T.-L. Ho, Phys. Rev. Lett. **107**, 210401 (2011).
[3] F. Wilczek and A. Zee, Proc. R. Soc. London, Sect. A **392**, 45 (1984).
[4] F. Wilczek and A. Zee, Phys. Rev. Lett. **52**, 2111 (1984).
[5] P. Wang, Z. Q. Yu, Z. Fu, J. Miao, L. Huang, S. Chai, H. Zhai, and J. Zhang, Phys. Rev. Lett. **109**, 095301 (2012).
[6] L. W. Cheuk, A. T. Sommer, Z. Hadzibabic, T. Yefsah, W. S. Bakr, and M. W. Zwierlein, Phys. Rev. Lett. **109**, 095302 (2012).
[7] Y.-J. Lin, K. Jimenez-Garcia, and I. B. Spielman, Nature (London) **471**, 83 (2011).
[8] Y.-J. Lin, R. L. Compton, A. R. Perry, W. D. Phillips, J. V. Porto, and I. B. Spielman, Phys. Rev. Lett. **102**, 130401 (2009).
[9] Y. J. Lin, R. L. Compton, K. Jimnez-Garca, J. V. Porto, and I. B. Spielman, Nature (London) **462**, 628 (2009).
[10] Y.-J. Lin, R. L. Compton, K. Jimenez-Garcia, W. D. Phillips, J. V. Porto, and I. B. Spielman, Nat. Phys. **7**, 531 (2011).
[11] Z. Q. Yu and H. Zhai, Phys. Rev. Lett. **107**, 195305 (2011).
[12] H. Hu, L. Jiang, X. J. Liu, and H. Pu, Phys. Rev. Lett. **107**, 195304 (2011).
[13] R. Liao, Y. Yi-Xiang, and W. M. Liu, Phys. Rev. Lett. **108**, 080406 (2012).
[14] J. P. Vyasanakere, S. Zhang, and V. B. Shenoy, Phys. Rev. B **84**, 014512 (2011).
[15] L. He and X. G. Huang, Phys. Rev. Lett. **108**, 145302 (2012).
[16] L. Han and C. A. R. Sáde Melo, Phys. Rev. A **85**, 011606(R) (2012).
[17] G. Chen, M. Gong, and C. Zhang, Phys. Rev. A **85**, 013601 (2012).
[18] A. Kubasiak, P. Massignan, and M. Lewenstein, Europhys. Lett. **92**, 46004 (2010).
[19] A. Bermudez, N. Goldman, A. Kubasiak, M. Lewenstein, and M. A. Martin-Delgado, New J. Phys. **12**, 033041 (2010).
[20] G. Liu, S. L. Zhu, S. Jiang, F. Sun, and W. M. Liu, Phys. Rev. A **82**, 053605 (2010).
[21] J. D. Sau, R. Sensarma, S. Powell, I. B. Spielman, and S. Das Sarma, Phys. Rev. B **83**, 140510 (2011).
[22] T. Fujita and K. F. Quader, Phys. Rev. B **36**, 5152 (1987).
[23] Y. Li and C. Wu, Phys. Rev. B **85**, 205126 (2012).
[24] N. F. Mott and H. S. W. Massey, *The Theory of Atomic Collisions*, 3rd ed. (Oxford University Press, London, 1965).
[25] A. Messiah, *Quantum Mechanics* (Wiley, New York, 1962).
[26] E. Braaten and H. W. Hammer, Phys. Rep. **428**, 259 (2006).
[27] T. Köhler and K. Góral, Rev. Mod. Phys. **78**, 1311 (2006).
[28] C. Chin, R. Grimm, P. Julienne, and E. Tiesinga, Rev. Mod. Phys. **82**, 1225 (2010).
[29] S. Inouye, M. R. Andrews, J. Stenger, H.-J. Miesner, D. M. Stamper-Kurn, and W. Ketterle, Nature (London) **392**, 151 (1998).
[30] P. Courteille, R. S. Freeland, and D. J. Heinzen, F. A. van Abeelen, and B. J. Verhaar, Phys. Rev. Lett. **81**, 69 (1998).
[31] J. L. Roberts, N. R. Claussen, J. P. Burke, C. H. Greene, E. A. Cornell, and C. E. Wieman, Phys. Rev. Lett. **81**, 5109 (1998).
[32] V. Vuletić, A. J. Kerman, C. Chin, and S. Chu, Phys. Rev. Lett. **82**, 1406 (1999).
[33] L. Pricoupenko and Y. Castin, Phys. Rev. A **69**, 051601(R) (2004).
[34] T. Bourdel, J. Cubizolles, L. Khaykovich, K. M. F. Magalhães, S. J. J. M. F. Kokkelmans, G. V. Shlyapnikov, and C. Salomon, Phys. Rev. Lett. **91**, 020402 (2003).
[35] J. W. Negele and H. Orland, *Quantum Many-Particle Systems* (Addison-Wesley, New York, 1988).
[36] D. S. Saraga and Daniel Loss, Phys. Rev. B **72**, 195319 (2005).
[37] G. D. Mahan, *Many-Particle Physics* (Plenum, New York, 1990).
[38] A. L. Fetter and J. D. Walecka, *Quantum Theory of Many Particle Systems* (McGraw-Hill, New York, 1971).
[39] C. Chin, M. Bartenstein, A. Altmeyer, S. Riedl, S. Jochim, J. H. Denschlag, and R. Grimm, Science **305**, 1128 (2004).
[40] C. H. Schunck, Y. Shin, A. Schirotzek, M. W. Zwierlein, and W. Ketterle, Science **316**, 867 (2007).
[41] M. Veillette, E. G. Moon, A. Lamacraft, L. Radzihovsky, S. Sachdev, and D. E. Sheehy, Phys. Rev. A **78**, 033614 (2008).
[42] D. S. Petrov, Phys. Rev. A **67**, 010703 (2003).
[43] J. P. D'Incao and B. D. Esry, Phys. Rev. Lett. **94**, 213201 (2005).
[44] H. Hu, H. Pu, J. Zhang, S. G. Peng, and X. J. Liu, Phys. Rev. A **86**, 053627 (2012).